Chemical Science

RSC Publishing

EDGE ARTICLE

View Article Online
View Journal | View Issue



Cite this: *Chem. Sci.*, 2013, **4**, 1625

# Denaturation of dsDNA immobilised at a negatively charged gold electrode is not caused by electrostatic repulsion†

Robert P. Johnson,[a] Nittaya Gale,[b] James A. Richardson,[a] Tom Brown[a] and Philip N. Bartlett*[a]

Received 4th December 2012
Accepted 22nd January 2013

DOI: 10.1039/c3sc22147d

**www.rsc.org/chemicalscience**

Double-stranded DNA immobilised through a thiol anchor at a gold electrode surface can be unwound and denatured by applying a negative potential. One proposed mechanism for this electrochemical denaturation is that electrostatic field effects are responsible for the destabilisation of the dsDNA through repulsion of the DNA sugar-phosphate backbone away from the electrode surface. Herein, we demonstrate conclusively that electrochemical melting at gold electrodes cannot be explained solely as a simple repulsion mechanism by showing that immobilised DNA denatures at high ionic strengths, where the DNA base-pairs are situated outside of the electrochemical double-layer (and outside the influence of the electric field), and further, that oligomers comprised of the mimic peptide nucleic acid (PNA) can also be denatured at negative potentials, despite the absence of a negatively charged backbone.

## Introduction

The first reported observation of electrochemical unwinding and denaturation of DNA at negative potentials was at a mercury drop electrode in 1974.[1,2] In the years since, potential driven changes in DNA conformation at the surfaces of mercury electrodes were studied extensively by the laboratories of Paleček[3–8] and Nurnberg.[9–12] A tentative scheme for DNA unwinding at negative electrode potentials was proposed based on electrostatic repulsion of the sugar-phosphate backbone of DNA.[2,4,8] In this scheme, DNA is absorbed at the electrode surface through the sugar phosphate backbone, and sporadically through hydrophobic base-pairs. As the potential is driven negative, the parts of the DNA adsorbed through the backbone desorb, whilst those parts attached through the base-pairs remain, resulting in unwinding and denaturation. This type of DNA unwinding was found to be dependent on nucleotide sequence.[13] Electrochemically induced denaturation has also been observed at graphite,[14] gold[15,16] and platinum electrodes.[17] At gold and platinum, the denaturation of dsDNA upon exposure to negative potentials was found to be dependent on the stability of duplex and was used to discriminate mismatched from fully complementary sequences. In these examples, a constant bias voltage was used, and because of the low magnitude of the applied voltage only partial denaturation (unwinding) was observed.[16,17]

In our recent work we have exploited complete electrochemically induced DNA denaturation, or electrochemical melting, to develop assays that are capable of differentiating between oligonucleotides based on their sequence and composition.[18–21] In a typical electrochemical melting assay a target nucleotide of interest is hybridised to a probe nucleotide immobilised at the surface of a nanostructured sphere segment void (SSV) substrate. The substrate is specifically designed to provide large ($\sim 10^7$) and reproducible Raman enhancement.[22,23] Typically, detection of DNA hybridisation is through a Raman label attached to the target nucleotide, although, we have recently demonstrated that hybridisation of un-labelled nucleotides can also be detected by exposing the immobilised duplex to a dsDNA specific binding molecule such as methylene blue.[24] Following hybridisation, the potential at the surface is driven negative, resulting in complete denaturation of the dsDNA, which is monitored through attenuation of the intensity of signal from the Raman label. The signal intensity drops during denaturation because the target nucleotide diffuses away from the surface. The SERS effect is surface selective; that is, enhancement of signal intensity occurs only within ~50 nm of the substrate surface. Using electrochemical melting, we have been able to discriminate mutations in the gene responsible for cystic fibrosis,[18] and to distinguish between short tandem repeats as used in criminal forensics from PCR products without the need for purification.[25] We have also demonstrated

[a]*Chemistry, University of Southampton, Southampton, SO17 1BJ, UK. E-mail: pnb@soton.ac.uk*

[b]*ATDBIO, University of Southampton, Southampton, SO17 1BJ, UK*

† Electronic supplementary information (ESI) available: Additional electrochemical melting data, structures of synthetic modifications made to DNA and PNA, full details of the synthesis of DNA and PNA, comparison of electrochemical melting potentials to our previous work. See DOI: 10.1039/c3sc22147d

that the potential required to induce denaturation is related to the sequence of the immobilised DNA, suggesting that electrochemical melting can be useful in a wide range of applications.[20]

In order to gain increased insight into the electrochemical unwinding and denaturation mechanism, we have recently studied the use of the electrostatically neutral DNA analogue peptide nucleic acid (PNA) in an electrochemical melting assay. PNA was first synthesised by Peter Nielsen and co-workers at the University of Copenhagen in 1991.[26] In PNA, nucleobases are linked by peptide bonds rather than a sugar-phosphate backbone. PNA/PNA and PNA/DNA duplexes are significantly more stable than their DNA/DNA counterparts of the same base-pair sequence because of the reduction in electrostatic repulsion between the complementary nucleotides.[27,28] For this reason, PNA has found a number of applications in molecular biology where there is a need to design probes that bind strongly to a complementary DNA target whilst keeping the probe as short as possible.[29,30] The properties of PNA mean that it has received extensive attention as a probe molecule in DNA detection assays, including those using electrochemical methods.[31–33]

Despite widespread use, there are few studies of the underlying electrochemistry of PNA,[31,34–36] and, to the best of our knowledge, electrochemical unwinding and denaturation of PNA/PNA duplexes and DNA/PNA hybrids under an applied potential has not previously been observed. The utilisation of PNA targets permits a possible mechanism for electrochemical melting unwinding and denaturation to be tested. If the denaturation process is driven purely by an electrostatic repulsion between the target strand and the negatively charged electrode surface, then PNA targets, which hold no formal charge, should remain hybridised complementary to an immobilised probe strand at the electrode surface as the potential is driven negative. In addition to providing a test of the denaturation mechanism, PNA has several advantages over DNA that may later prove useful in the development of electrochemical melting assays. Firstly, PNA/DNA chimera are significantly more stable than DNA/DNA duplexes of the same sequence,[37] and therefore defects in structure such as base-pair mismatches are more easily detected relative to the perfectly complementary.[27,28] Further, an immobilised PNA probe strand is likely to be significantly more stable than a DNA probe strand under an applied potential because there will be no repulsion between the neutral backbone of the PNA and the electrode surface. Rant *et al.* have demonstrated previously that repulsion between the sugar-phosphate backbone of thiol-anchored ssDNA and the electrode surface makes a significant contribution to reductive desorption of the DNA,[38] and thus, electrochemical melting assays that utilise immobilised PNA probes are likely to prove more robust.

## Experimental

### Preparation of Sphere Segment Void (SSV) substrates

A gold-chrome coated microscope slide was prepared by thermal vapour deposition of a 10 nm chromium adhesion layer followed by approximately 200 nm gold onto a standard glass microscope slide (76 mm × 26 mm × 1 mm). A monolayer template of 600 nm of polystyrene spheres (Fisher Scientific as a 1 wt% aqueous suspension) was formed at the surface using a convective assembly method described by our group previously.[23] Gold was deposited through the template to a height of 480 nm at −0.72 V *vs.* saturated calomel electrode (SCE) from a commercial cyanide free gold plating solution (Metalor, ECF 60) containing an additive (Metalor, Brightener E3) to leave a bright and smooth finish. Following electrodeposition, the polystyrene spheres were removed by dissolving in DMF (Rathburn, HPLC) and the substrates rinsed thoroughly with water.

### Oligonucleotide and PNA synthesis

DNA and PNA synthesis was performed using standard methods at ATDBio, Southampton, United Kingdom. A full description of the synthetic methodology and structural modifications are given in the ESI.† The sequence used for both the DNA and PNA probes was 5′-ATA GAC TGT CCG, with a 5′ thiol anchor modification (Fig. S1†). The DNA or PNA target sequence labelled with Cy3 at the 3′ (Fig. S2†) was the fully complementary sequence. The thiol anchors utilised are stable over the potential ranges used in this work (up to −1200 mV *vs.* Ag/AgCl), as demonstrated for the DNA anchor in previous publications,[18,21] and shown for the PNA anchor in Fig. S6.†

### Immobilisation and hybridisation protocol

To perform the immobilisation of DNA, substrates were immersed into a 10 mM Tris buffer (pH 7.2) containing 1 M NaCl and 1 μM of the di-thiol modified DNA strand for 12 h. For the immobilisation of PNA, the immobilisation buffer consisted of 1 μM of the di-thiol modified PNA in water with 5% DMSO by volume (Rathburn, HPLC) to facilitate complete dissolution of the modified PNA, and 10 mM mercaptohexanol (98%, Sigma-Aldrich) to ensure a surface coverage of the same order of magnitude as is normally obtained for DNA. The addition of mercaptohexanol to the DNA immobilisation buffer is necessary because of the smaller footprint of the PNA thiol anchor (Fig. S1†), which would otherwise permit a much larger surface coverage. In both cases following immobilisation, the remaining gold surface was passivated by immersing the substrate in a 10 mM Tris buffer (pH 7.2) containing 1 M NaCl and 10 mM mercaptohexanol for 20 min. After passivation, the substrates were rinsed thoroughly and stored in buffer solution until required.

Hybridisation of Cy3-labelled DNA was achieved by immersing the substrate into a 10 mM Tris buffer (pH 7.2) containing 1 M NaCl and 1 μM of the DNA target. The same procedure was used for the immobilisation of PNA, except that immobilisation buffer consisted of 5% DMSO (Rathburn, HPLC) to facilitate complete dissolution of the Cy3 labelled target. Substrates were rinsed thoroughly with buffer before use in an electrochemical melting experiment.

### Surface coverage determination

The surface coverage of the immobilised oligonucleotides was determined using the coulometric method described by Steel

 

and co-workers.[39] A three electrode system was used for the measurements, where the DNA covered SSV surface and a platinum gauze were used as the working and counter electrodes respectively. An SCE was used as the reference. A 500 ms pulse at −400 mV *vs.* SCE was applied from an initial potential of 100 mV in the presence and absence of ruthenium hexamine. The supporting electrolyte used was a 10 mM Tris (pH 7.2) buffer which was purged with argon for 30 min and blanketed with argon thereafter.

### Electrochemical melting procedure

Electrochemical melting experiments were carried out in a custom built spectro-electrochemical Raman cell (Ventacon Ltd.) specifically designed for use with a Renishaw 2000 Raman microscope. It utilises a horizontal geometry for viewing under the microscope, maintaining a thin 150 μl liquid film on the substrate. Electrochemical control is provided by a three electrode arrangement inside the cell, where the substrate is used as the working electrode, and a platinum wire as the counter and a silver/silver chloride as the reference. In a typical electrochemical melting experiment the potential was swept at 0.5 mV $s^{-1}$ from a starting potential of −0.4 V up to −1.6 V in a 10 mM Tris buffer with added NaCl. The total ionic strength was either 0.01, 0.1 or 1 M. All electrochemical measurements were carried out using an EcoChemie μAutolabIII potentiostat/galvanostat at room temperature.

### Raman instrumentation

Raman spectra were acquired using a 50× objective on a Renishaw 2000 microscope instrument equipped with a 632.8 nm He–Ne laser and Prior XYZ stage controller. The diameter of the laser spot was 1 μm. Typically, Raman spectra were acquired from a 10 × 10 μm area with the laser moved approximately 2 μm between measurements in order to avoid bleaching effects. Typically, a single 30 s acquisition was used to acquire spectra.

### Data analysis

SERS spectra presented have been baseline corrected using a polynomial multipoint fitting function and curve-fitting performed as required with Renishaw WiRe 3.1. The Raman intensities of the peaks are taken as height above the baseline. A Boltzmann function was used to fit sigmoidal curves to the melting profiles (Origin 8.6) and the mid point of the sigmoidal curves were used to determine the melting potential, along with the associated standard error.

## Results

### Probe design, immobilisation and characterisation

Two PNA and two DNA oligomers were synthesised such that it was possible to produce all four possible combinations of probe and target strands at the substrate surface (Fig. 1). The probes were designed to bind to the gold substrates through three dithiol groups attached to the probe oligonucleotide on the 5′ end and three cysteine residues attached to the PNA *N*-terminus. The target strands were all labelled with Cy3 at the 3′ end of the DNA and carboxy-terminus of the PNA, such that the label was proximal to the surface. This maximises the SERS signal because the intensity of the signal attenuates as a function of distance from the surface. Structures of the oligonucleotide and PNA modifications are given in the ESI.† During design, particular consideration was given to the GC content of the oligomers, because high GC content significantly decreases the solubility of PNA strands in aqueous media. Despite this, we found that it was necessary to add dimethyl sulfoxide (DMSO) to the PNA-containing immobilisation and hybridisation buffers in order to compensate for the decrease in solubility caused by the addition of the thiol-anchor and label modifications to the PNA. Immobilisation and hybridisation buffers for PNA contained 5% DMSO by volume. Whilst DNA containing buffers consisting of just salt and water were found to be consistently stable, buffers that had added DMSO became unstable after a few days as the co-solvent became immiscible over an extended period of time.

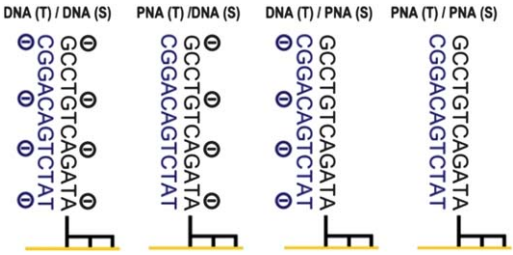


**Fig. 1** Sequences of the four possible combinations of DNA and PNA studied at the electrode surface (S is probe strand and T is target strand).

The surface density of DNA probes at a gold electrode were estimated using a chronoamperometric method published by Steel and co-workers.[39] Reductive pulses were applied to a nanostructured gold substrate in the presence and absence of the redox probe ruthenium(III) hexamine, which displaces NaCl bound to DNA, and, under conditions of saturation, can be used to deduce the probe surface density as has been described previously. We found the surface coverage of immobilised ssDNA to be $1.02 \times 10^{12}$ molecules per $cm^2$ ($[Ru(NH_3)_6^{3+}] = 25$ μM, electrode area 0.17 $cm^{-2}$), which is consistent with previous results from our group, obtained using the same immobilization protocols and probes with the same thiol anchor.[18]

Given the lack of charge on the backbone of PNA, and the different structure of the thiol anchor used to immobilize the PNA probes at the electrode surface (Fig. S1†), we anticipated the surface coverage of PNA at the surface in our experiments to be different. To characterize the surface density of PNA, we first exposed the immobilised PNA probes to fully complementary DNA for 12 h, and then carried out the chronoamperometric experiments in the presence and absence of ruthenium hexamine in the same way as described above for the DNA probes. We found that the surface coverage of immobilised PNA to be $3.74 \times 10^{12}$ molecules per $cm^2$ (Fig. 2), notably higher than the results obtained for DNA. It is probable that the lack of charge on the backbone of PNA means that adsorbing strands do not repel one another as they adsorb on the surface, resulting in a

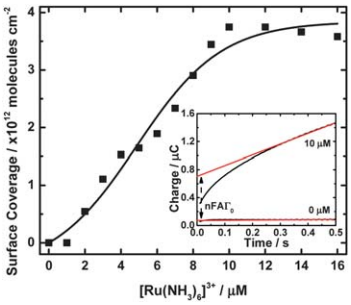


**Fig. 2** Binding isotherm for the interaction of $[Ru(NH_3)_6]^+$ with DNA hybridised to fully complementary PNA which is immobilised at a sphere segment void surface. Inset: colorimetric curves were recorded by stepping the potential from 0.1 to −0.4 V *vs.* SCE at a PNA coated electrode bound to fully complementary DNA targets in a 10 mM Tris (pH 7.2) buffer The area of the electrode was 0.26 $cm^2$.

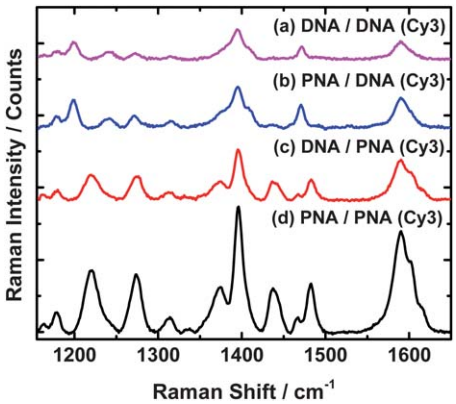


**Fig. 3** Detection of DNA and PNA duplexes at the surface of a sphere segment void substrate. (a) DNA/DNA(Cy3) (b) PNA/DNA(Cy3) (c) DNA/PNA(Cy3) (d) PNA/PNA(Cy3). Utilising PNA instead of DNA for the probe results in a ∼2× increase in spectral intensity (compare a and b). Replacing a Cy-3 labelled DNA target strand with Cy-3 labelled PNA results in an increase in spectral intensity, in addition to changes in the observed bands (compare a and c). Spectra were recorded with a single 30 s acquisition at a potential of −450 mV in a 10 mM Tris (pH 7.2) buffer with added NaCl ($I$ = 0.1 M) and are presented baseline corrected.

higher surface density. The lack of backbone charge has also been attributed to the strong adsorption of PNA at mercury[34,35] and carbon electrodes.[34] We note however that the surface densities obtained for PNA using the chronoamperometric method described here can only be considered as an estimate, as it is impossible to demonstrate conclusively that all of the PNA probes are bound to a DNA target (meaning that the true surface coverage may well be greater than reported here), nor that the PNA/DNA duplex interacts with ruthenium hexamine in the same manner as a immobilised DNA molecule.

### SERS detection of DNA and PNA

Complementary oligomers of either DNA or PNA were bound to the immobilised probe strand by exposing the substrate to a 1 μM solution of the desired target for 12 h, followed by thorough rinsing with buffer solution. Binding of the complementary oligomer of either DNA or PNA, which was in all cases labelled with Cy3, was determined by acquiring the surface enhanced Raman spectra.

We found the order of intensity of the spectra acquired under the same conditions for the different duplex combinations to vary in the order

$$\text{DNA(S)/DNA(T)} < \text{PNA(S)/DNA(T)} < \text{DNA(S)/PNA(T)} \ll \text{PNA(S)/PNA(T)}$$

as shown in Fig. 3. The higher SERS intensities observed when PNA probes are utilised can easily be attributed to the higher surface densities for these systems, as shown through the chronoamperometric experiments presented earlier. Utilising a PNA probe instead of DNA results in a ∼2× increase in spectral intensity (compare a and b). The higher SERS intensities observed for systems in which Cy3 labelled PNA targets are utilised is more complex. We suggest that the orientation of the Cy3 dye relative to the surface, which is likely different depending on whether the Cy3 is attached to DNA or PNA, is responsible for the differences observed in intensity. This theory is supported by notable differences in relative intensities and positions of the bands in the recorded spectra (Fig. 3). For example, the band at 1190 $cm^{-1}$ appears only when Cy3 is attached to DNA, whilst the band 1220 $cm^{-1}$ appears only when Cy3 is attached to PNA. Further, the bands at 1240 $cm^{-1}$ and 1470 $cm^{-1}$ are significantly more intense where Cy3 is attached to DNA rather PNA, whilst the reverse is true of the bands at 1437 $cm^{-1}$ and 1480 $cm^{-1}$. Given that Cy3 is positively charged, and the linker through which it is attached to either the DNA or PNA is flexible (Fig. S2†), it is entirely plausible that there will be differences in the interaction and thus the favoured orientation of the dye depending on whether the nucleic acid to which it is attached is either charged (DNA) or uncharged (PNA). Further, Cy3 is also well known to interact specifically with DNA duplexes through stacking interactions with the terminal base-pairs,[40–44] and thus the consequences of the duplex construction (either DNA or PNA) on Cy3 orientation cannot be ignored.

### Electrochemical melting of DNA and PNA duplexes

Electrochemical melting experiments were performed using each of the four possible nucleotide combinations. In each experiment, after hybridisation with the target, the potential was ramped at 0.5 mV $s^{-1}$ from a starting potential of −0.3 V to a final potential of −1.6 V *vs.* Ag/AgCl. SERS spectra were recorded at 25 mV intervals.

A simple electrostatic repulsion mechanism for oligomer denaturation at an electrode surface suggest that it should be impossible to denature those duplexes which contained a non-anchored PNA strand because of the absence of charge on the oligomer backbone. However, electrochemical denaturation of an all-PNA duplex proved easily possible at moderately cathodic potentials. The potential required to denature the PNA duplex was similar to that required to electrochemically denature a DNA/DNA duplex of identical composition (Fig. 4).

We performed electrochemical melting experiments for all four possible combinations of DNA and PNA at the surface, at

 

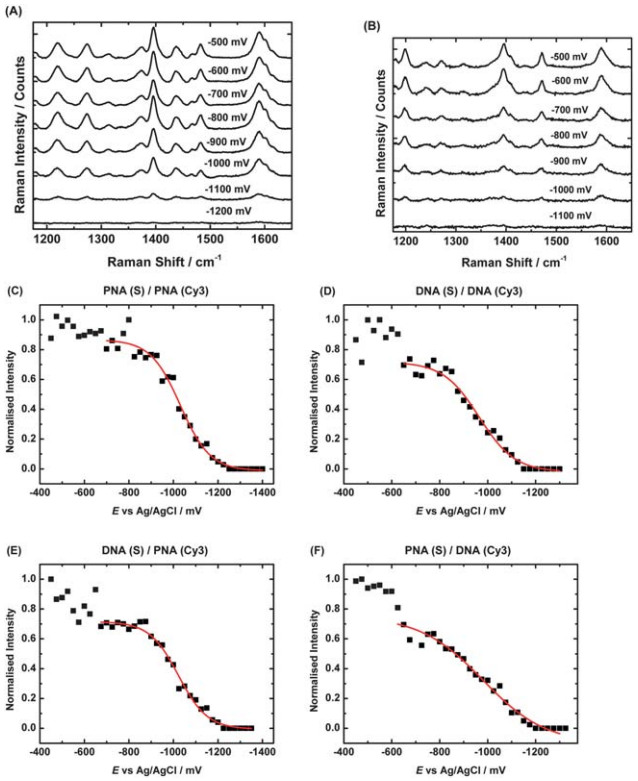


**Fig. 4** Electrochemical melting of duplexes constructed of DNA and/or PNA at a sphere segment void surface. Representative spectra for the case of (A) PNA/PNA(Cy3) and (B) DNA/DNA(Cy3), and the peak intensity at 1590 $cm^{-1}$ for (C) PNA/PNA(Cy3), (D) DNA/DNA(Cy3), (E) DNA/PNA(Cy3) and (F) PNA/DNA(Cy3) as a function of the applied potential. Sigmoidal curves have been fitted to the region corresponding to denaturation of duplex. The potential was swept at a scan rate of 0.05 mV $s^{-1}$ in a 10 mM Tris buffer (pH 7.2) with added NaCl ($I = 0.1$ M). Spectra were acquired with a 2.7 mW 633 nm excitation laser and have been background subtracted and normalized to maximum.

three different ionic strengths; 0.01, 0.1 and 1 M. It was possible to denature the immobilised duplexes in all cases. Denaturation of the duplexes was monitored through attenuation of the band at 1593 $cm^{-1}$, attributed to the C=N chromophore stretch, and the attenuation of signal plotted as a function of the potential. Data obtained at an ionic strength of 0.1 M are shown in Fig. 4. Unlike the Texas Red labelled oligonucleotides presented in our previous work,[20] no initial rise in intensity was observed upon driving the potential negative. Instead, for the Cy3 labelled oligomers used here, we observed a decrease in signal before a plateau is reached, which suggests that label re-orientates in a position away from the surface as the potential is driven negative. It is possible that this re-orientation affect is responsible for the greater fluctuation in intensity values observed at less negative potentials, where the position and orientation of the Cy3 label relative to the substrate surface stabilises as the potential becomes more negative. The onset of electrochemical denaturation was similar regardless of the construction of the probe or target, at approximately −700 mV. Melting potentials for the duplexes, determined from the first derivative of the sigmoidal fit, are shown in Table 1.

**Table 1** Melting potentials of the nucleic acid duplexes studied (determined from the mid-point of the sigmoidal fit to melting region as shown in Fig. 4, S3 and S4). Determination of the $T_m$ values is shown in Fig. S7.

| Probe<br>Target | DNA<br>DNA(Cy3) | PNA<br>DNA(Cy3) | DNA<br>PNA(Cy3) | PNA<br>PNA(Cy3) |
|---|---|---|---|---|
| $T_m$ (0.1 M)/°C | 47 | 63 | 67 | >80 |
| $E_m$ (0.01 M)/mV | $-1030 \pm 17$ | $-1050 \pm 13$ | $-1097 \pm 13$ | $-1130 \pm 15$ |
| $E_m$ (0.1 M)/mV | $-963 \pm 9$ | $-979 \pm 20$ | $-1007 \pm 12$ | $-1024 \pm 16$ |
| $E_m$ (1 M)/mV | $-890 \pm 38$ | $-910 \pm 26$ | $-953 \pm 9$ | $-985 \pm 17$ |

At all three ionic strengths, the melting potentials became progressively more negative in the same order as would be expected based on the experimentally determined melting temperatures in solution at 0.1 M for the four combinations of DNA and PNA. However, there are a number of aspects of the determined melting potentials that are puzzling. Firstly, PNA duplexes appears to denature at cathodic potentials not significantly different from DNA duplexes, despite the huge differences in melting temperature, suggesting that the potential required to achieve denaturation is not directly related to the thermodynamic stability. Whilst the melting potential for the DNA/DNA duplex is close to that which would be predicted based on our previously developed model, the melting potentials of the PNA containing duplexes are much less negative than expected (Fig. S5†). For example, the PNA/PNA duplex, which had a melting temperature outside the range of our instrumentation (>80 °C), had a melting potential only *circa* 100 mV negative of the DNA/DNA duplex of identical base-pair composition. The way in which the melting potentials vary with the ionic strength is also surprising. Whilst PNA containing duplexes destabilise with increasing ionic strength,[37] double-stranded DNA is well known to increase in thermodynamic stability with increasing ionic strength.[45] However, the results here clearly showed a trend to less negative potentials with increasing ionic strength in electrochemical melting. It is worth noting that a similarly unexpected trend was observed by Paleček and Ostatna for the denaturation of BSA at mercury electrodes,[46] and it something that we intend to explore in more detail for DNA at a later stage. From the results presented here, it is clear that PNA duplexes can be denatured at a negatively charged electrode surface at potentials similar to those that are required to denature double-stranded DNA, despite the lack of charge on the backbone of PNA.

## Mechanisms for denaturation at negative potentials

For electrostatic repulsion to be a plausible mechanism for electrochemically induced unwinding and denaturation in our experiments, those duplexes in which the non-immobilised oligomers were constructed from PNA should have been stable under an applied negative potential. This is because, under the neutral pH regime used here (pH 7.2), the backbone of PNA has no formal charge, and, unlike DNA at an electrode surface, will experience no electrostatic effect under an applied electric field. Nevertheless, we observed electrochemical unwinding and denaturation of DNA/PNA and PNA/PNA duplexes at negative

potentials. Whilst an indirect mechanism of electrostatic repulsion might still hold for the case of the immobilised DNA and the PNA target through an indirect repulsion of the immobilised strand, electrostatic repulsion does not serve as a plausible explanation for the observed denaturation of duplexes comprising entirely of PNA. We have demonstrated previously that nucleic acid sequence[20] and the presence or absence of mismatches[18,24] is related to the magnitude of the potential required to drive denaturation. Whilst we found this was also the case here, the magnitude of potential required to drive denaturation was much lower than would be expected based on our previously developed model[20] (Fig. S5†). This is in sharp contrast to the well-known increased thermodynamic stability of duplexes that contain PNA,[27] suggesting that whilst electrochemical denaturation in our assays is related to the base-pair composition, this does not extend to the composition of the nucleic acid backbone. Any simple relationship between the potential required to electrochemically denature immobilised DNA in our assay and thermodynamic properties of that duplex is therefore unlikely.

In the course of extensive studies of DNA electrochemistry at mercury drop electrodes, Paleček and Jelen observed DNA unwinding at ionic strengths of between 0.1 and 1 M NaCl, and in common with our studies, found that the denaturation was highly dependent on the base-pair sequence.[13] They proposed a tentative scheme based on an electrostatic repulsion.[4,7] In their experiments, DNA is adsorbed at the electrode surface in some parts *via* the hydrophobic individual bases, and in other parts through the sugar-phosphate backbone. Upon driving the potential negative, those parts that are not bound through the bases will be repelled away from the surface, resulting in a stress force on the DNA that might be responsible for the unwinding. It is important to note that, under these conditions, where the sugar-phosphate backbone is adsorbed directly at the electrode surface, the DNA is likely to experience strong electrostatic forces even at high ionic strengths. Thus, even though the results presented here preclude a simple electrostatic repulsion mechanism as an explanation for electrochemical unwinding and denaturation in our experiments, the mechanism proposed by earlier by Paleček *et al.* is still plausible for the regime of DNA directly adsorbed at mercury electrodes.[4,7]

Additional evidence discounting electrostatic repulsion as a possible mechanism for electrochemical unwinding and denaturation in our system can be inferred from the observation of electrochemically induced denaturation even at high ionic strength. For our system, in which the dsDNA is immobilised at the gold electrode through a thiol group at the terminus, the conformation adopted at a gold surface by thiolated dsDNA is upright where the base pairs are situated near-perpendicular with respect to the electrode surface. This has been confirmed in the literature by numerous experimental techniques, including atomic force microscopy,[47] fluorescence,[48,49] X-Ray photoelectron spectroscopy[50] and surface plasmon resonance.[51] Under regimes of high ionic strength, and given the upright conformation adopted by the dsDNA at the surface, the effective electric field experienced by the sugar phosphate backbone is likely to be negligible. This is because the sugar-phosphate backbone is anticipated to fall outside of the electrochemical double layer (EDL), where the majority of the electric field is compensated by ions from the electrolyte over a distance shorter than between the electrode surface and the first base-pair of the immobilised DNA (Fig. 5).

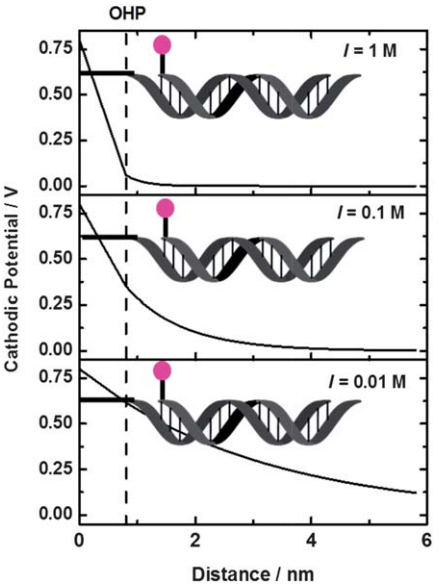


**Fig. 5** Potential profile of the electrical double layer at different ionic strengths and a cathodic potential of 0.8 V based on the Gouy–Chapman–Stern model with an outer-helmholtz plane at ~0.8 nm. The 12 base-pair dsDNA molecule (~4 nm) attached to the surface by the thiol anchor group (~1 nm) is overlain for comparison. At high ionic strength all of the dsDNA base-pairs are situated outside of the double layer. In this model we have ignored the mercaptohexanol monolayer.

Previously, we have been able to discount a number of plausible explanations, including, here, electrostatic repulsion, and in our earlier work, localised pH changes at the vicinity of the electrode surface[21] as suggested by Sosnowski and co-workers as a possible mechanism.[17] Another plausible mechanism for DNA and PNA denaturation at a negatively charged electrode surface is the disruption of base stacking and/or hydrogen bonding between nucleobases upon an increase in electron density into the (pseudo)nucleic acid π-stack. The stabilising effect of electron withdrawing groups on the π–π stacking interaction of simple aromatic molecules has previously been demonstrated[52,53] and recent studies on the modification of RNA with 2′-deoxy-2′fluoro groups suggests that electron withdrawing substituents can increase the thermodynamic stability of this nucleic acid duplex.[54,55] Thus, a mechanism by which denaturation of DNA or PNA is brought about *via* the donation of electron density from a negatively charged surface into the duplex may provide an explanation.

Clearly, further work is required to fully understand the mechanism for electrochemical denaturation at gold electrode surfaces. Nevertheless, electrochemical melting offers great potential for use in diagnostic assays. In particular, the use of PNA probe molecules can be exploited to improve the robustness of our assays through increased stability of the probe at the electrode surface and the ability to access a wider range of target sequences that would otherwise be unstable at room-temperatures.

## Conclusions

We have demonstrated that immobilised oligonucleotides of both DNA and PNA can be unwound at an electrode surface at negative potentials. Denaturation of duplexes comprised of entirely PNA occurs despite the absence of backbone charge, strongly suggesting that the mechanism of DNA denaturation at electrodes cannot be a simple electrostatic repulsion. Further evidence ruling out an electrostatic repulsion mechanism is observed from electrochemical melting experiments at high ionic strength, where immobilised dsDNA is anticipated to fall outside of the electrical double layer and thus the influence of the applied electric field.

## Notes and references

1 P. Valenta and H. W. Nürnberg, *Eur. Biophys. J.*, 1974, **1**, 17–26.
2 E. Palecek, *Collect. Czech. Chem. Commun.*, 1974, **39**, 3449–3460.
3 M. Bartošík and E. Paleček, *Electroanalysis*, 2011, 1311–1319.
4 E. Palecek and F. Jelen, in *Electrochemistry of Nucleic Acids and Protiens – Towards Electrochemical Sensors for Genomics and Proteomics*, ed. E. Palecek, F. Scheller and J. Wang, Elsevier, Amsterdam, 2005, ch. 3.
5 E. Paleček and S. Kwee, *Collect. Czech. Chem. Commun.*, 1979, **44**, 448–455.
6 E. Palecek, *Bioelectrochem. Bioenerg.*, 1992, **28**, 71–83.
7 E. Paleček and M. Bartošík, *Chem. Rev.*, 2012, 3427–3481.
8 V. Brabec and E. Palecek, *Biophys. Chem.*, 1976, **4**, 79–92.
9 H. W. Nurnberg and P. Valenta, in *Ions in Macromolecular and Biological Systems*, Scientechnica, Bristol, 1977, p. 201.
10 P. Valenta and P. Grahmann, *J. Electroanal. Chem.*, 1974, **49**, 41–53.
11 P. Valenta and H. W. Nürnberg, *J. Electroanal. Chem.*, 1974, **49**, 55–75.
12 P. Valenta, H. W. Nürnberg and P. Klahre, *Bioelectrochem. Bioenerg.*, 1974, **1**, 487–505.
13 F. Jelen and E. Palecek, *Gen. Physiol. Biophys.*, 1985, **2**, 219–237.
14 V. Brabec, V. Vetterl and O. Vrana, in *Bioelectrochemistry: Principles and Practice*, ed. V. Brabec, D. Walz and G. Milazzo, Birkhauser Verlag, Basel, Switzerland, 1996, vol. 3.
15 A.-M. Spehar-Deleze, L. Schmidt, R. Neier, S. Kulmala, N. de Rooij and M. Koudelka-Hep, *Biosens. Bioelectron.*, 2006, **22**, 722–729.
16 R. J. Heaton, A. W. Peterson and R. M. Georgiadis, *Proc. Natl. Acad. Sci. U. S. A.*, 2001, **98**, 3701–3704.
17 R. G. Sosnowski, E. Tu, W. F. Butler, J. P. O'Connell and M. J. Heller, *Proc. Natl. Acad. Sci. U. S. A.*, 1997, **94**, 1119–1123.
18 S. Mahajan, J. Richardson, T. Brown and P. N. Bartlett, *J. Am. Chem. Soc.*, 2008, **130**, 15589–15601.
19 S. Mahajan, J. Richardson, N. B. Gaied, Z. Zhao, T. Brown and P. N. Bartlett, *Electroanalysis*, 2009, **21**, 2190–2197.
20 R. P. Johnson, R. Gao, T. Brown and P. N. Bartlett, *Bioelectrochemistry*, 2012, **85**, 7–13.
21 R. P. Johnson, J. A. Richardson, T. Brown and P. N. Bartlett, *Langmuir*, 2012, **28**, 5464–5470.
22 R. P. Johnson, S. Mahajan, M. E. Abdelsalam, R. M. Cole, J. J. Baumberg, A. E. Russell and P. N. Bartlett, *Phys. Chem. Chem. Phys.*, 2011, **13**, 16661–16665.
23 S. Mahajan, R. M. Cole, B. F. Soares, S. H. Pelfrey, A. E. Russell, J. J. Baumberg and P. N. Bartlett, *J. Phys. Chem. C.*, 2009, **113**, 9284–9289.
24 R. P. Johnson, J. A. Richardson, T. Brown and P. N. Bartlett, *J. Am. Chem. Soc.*, 2012, **134**, 14099–14107.
25 D. K. Corrigan, N. Gale, T. Brown and P. N. Bartlett, *Angew. Chem.*, 2010, **122**, 6053–6056.
26 P. Nielsen, M. Egholm, R. Berg and O. Buchardt, *Science*, 1991, **254**, 1497–1500.
27 P. E. Nielsen and G. Haaima, *Chem. Soc. Rev.*, 1997, **26**, 73–78.
28 P. E. Nielsen and M. Egholm, *Curr. Issues Mol. Biol.*, 1999, **1**, 89–104.
29 T. T. Nikiforov and S. Jeong, *Anal. Biochem.*, 1999, **275**, 248–253.
30 K. Petersen, U. Vogel, E. Rockenbauer, K. Vang Nielsen, S. Kølvraa, L. Bolund and B. Nexø, *Mol. Cell. Probes*, 2004, **18**, 117–122.
31 E. Paleček, M. Trefulka and M. Fojta, *Electrochem. Commun.*, 2009, **11**, 359–362.
32 A. Macanovic, C. Marquette, C. Polychronakos and M. F. Lawrence, *Nucleic Acids Res.*, 2004, **32**, e20.
33 D. K. Corrigan, H. Schulze, G. Henihan, I. Ciani, G. Giraud, J. G. Terry, A. J. Walton, R. Pethig, P. Ghazal, J. Crain, C. J. Campbell, A. R. Mount and T. T. Bachmann, *Biosens. Bioelectron.*, 2012, **34**, 178–184.
34 M. Tomschik, F. Jelen, L. Havran, L. Trnková, P. E. Nielsen and E. Paleček, *J. Electroanal. Chem.*, 1999, **476**, 71–80.
35 M. Fojta, V. Vetterl, M. Tomschik, F. Jelen, P. Nielsen, J. Wang and E. Palecek, *Biophys. J.*, 1997, **72**, 2285–2293.
36 J. Wang, G. Rivas, X. Cai, M. Chicharro, N. Dontha, D. Luo, E. Palecek and P. E. Nielsen, *Electroanalysis*, 1997, **9**, 120–124.
37 S. Tomac, M. Sarkar, T. Ratilainen, P. Wittung, P. E. Nielsen, B. Nordén and A. Gräslund, *J. Am. Chem. Soc.*, 1996, **118**, 5544–5552.
38 U. Rant, K. Arinaga, T. Fujiwara, S. Fujita, M. Tornow, N. Yokoyama and G. Abstreiter, *Biophys. J.*, 2003, **85**, 3858–3864.
39 A. B. Steel, T. M. Herne and M. J. Tarlov, *Anal. Chem.*, 1998, **70**, 4670–4677.
40 J. Ouellet, S. Schorr, A. Iqbal, T. J. Wilson and D. M. J. Lilley, *Biophys. J.*, 2011, **101**, 1148–1154.
41 D. G. Norman, R. J. Grainger, D. Uhrín and D. M. J. Lilley, *Biochemistry*, 2000, **39**, 6317–6324.
42 A. Iqbal, S. Arslan, B. Okumus, T. J. Wilson, G. Giraud, D. G. Norman, T. Ha and D. M. J. Lilley, *Proc. Natl. Acad. Sci. U. S. A.*, 2008, **105**, 11176–11181.
43 B. J. Harvey, C. Perez and M. Levitus, *Photochem. Photobiol. Sci.*, 2009, **8**, 1105–1110.
44 A. Iqbal, L. Wang, K. C. Thompson, D. M. J. Lilley and D. G. Norman, *Biochemistry*, 2008, **47**, 7857–7862.

45 R. Owczarzy, Y. You, B. G. Moreira, J. A. Manthey, L. Huang, M. A. Behlke and J. A. Walder, *Biochemistry*, 2004, **43**, 3537–3554.
46 E. Paleček and V. Ostatna, *Chem. Commun.*, 2009, 1685–1687.
47 D. Erts, B. Polyakov, H. Olin and E. Tuite, *J. Phys. Chem. B.*, 2003, **107**, 3591–3597.
48 J. N. Murphy, A. K. H. Cheng, H.-Z. Yu and D. Bizzotto, *J. Am. Chem. Soc.*, 2009, **131**, 4042–4050.
49 W. Kaiser and U. Rant, *J. Am. Chem. Soc.*, 2010, **132**, 7935–7945.
50 T. M. Herne and M. J. Tarlov, *J. Am. Chem. Soc.*, 1997, **119**, 8916–8920.
51 K. A. Peterlinz, R. M. Georgiadis, T. M. Herne and M. J. Tarlov, *J. Am. Chem. Soc.*, 1997, **119**, 3401–3402.
52 S. L. Cockroft, C. A. Hunter, K. R. Lawson, J. Perkins and C. J. Urch, *J. Am. Chem. Soc.*, 2005, **127**, 8594–8595.
53 S. L. Cockroft, J. Perkins, C. Zonta, H. Adams, S. E. Spey, C. M. R. Low, J. G. Vinter, K. R. Lawson, C. J. Urch and C. A. Hunter, *Org. Biomol. Chem.*, 2007, **5**, 1062–1080.
54 M. Manoharan, A. Akinc, R. K. Pandey, J. Qin, P. Hadwiger, M. John, K. Mills, K. Charisse, M. A. Maier, L. Nechev, E. M. Greene, P. S. Pallan, E. Rozners, K. G. Rajeev and M. Egli, *Angew. Chem., Int. Ed.*, 2011, **50**, 2284–2288.
55 A. Patra, M. Paolillo, K. Charisse, M. Manoharan, E. Rozners and M. Egli, *Angew. Chem., Int. Ed.*, 2012, **51**, 11863–11866.

 